Intensity Dependent Photoluminescence Imaging for In-Line Quality Control of Perovskite Thin Film Processing

Benjamin Hacene, Felix Laufer, Simon Ternes, Ahmed Farag, Ronja Pappenberger, Paul Fassl, Somayeh Moghadamzadeh, Bahram Abdollahi Nejand, Thomas Feeney, Ian Howard, and Ulrich W. Paetzold*

Large area fabrication of high-quality polycrystalline perovskite thin films remains one of the key challenges for the commercial readiness of perovskite photovoltaic (PV). To enable high-throughput and high-yield processing, reliable and fast in-line characterization methods are required. The present work reports on a non-invasive characterization technique based on intensity-dependent photoluminescence (PL) imaging. The change in PL intensity as a function of excitation power density can be approximated by a power-law with exponent k, which is a useful quality indicator for the perovskite layer, providing information about the relative magnitudes of radiative and non-radiative recombination. By evaluating k-parameter maps instead of more established PL intensity images, 2D information is obtained that is robust to optically induced artifacts such as intensity variations in excitation and reflection. Application to various half stacks of a perovskite solar cell showcase its ability to determine the importance of the interface between the charge transporting and perovskite layers. In addition, the k-parameter correlates to the bulk passivation concentration, enabling rapid assessment of open-circuit voltage variations in the range of 20 mV. Considering expected improvements in data acquisition speed, the presented k-imaging method will possibly be obtained in real-time, providing large-area quality control in industrial-scale perovskite PV production.

B. Hacene, F. Laufer, S. Ternes, A. Farag, T. Feeney, I. Howard,
U. W. Paetzold
Light Technology Institute (LTI)
Karlsruhe Institute of Technology (KIT)
Engesserstrasse 13, 76131 Karlsruhe, Germany
E-mail: ulrich.paetzold@kit.edu
S. Ternes, A. Farag, R. Pappenberger, P. Fassl, S. Moghadamzadeh, B. A. Nejand, I. Howard, U. W. Paetzold
Institute of Microstructure Technology (IMT)
Karlsruhe Institute of Technology (KIT)
Hermann-von-Helmholtz-Platz 1, 76344 Eggenstein-Leopoldshafen, Germany

1. Introduction

Progress in photovoltaics (PV) is one of the pillars for accelerating the global transition to a sustainable energy production.[1] In the last decade, interest in hybrid perovskite semiconductors has increased rapidly given their excellent optoelectronic properties. Perovskite materials possess an outstanding defect tolerance, enabling long charge carrier lifetimes and diffusion lengths in polycrystalline thin films.[2,3] The bandgap of hybrid perovskites can be tuned over a wide range from 1.2 eV to 2.4 eV via their stochiometric composition, which is a major advantage of perovskites for application in tandem architectures.[4] However, the technology faces three major challenges that hamper commercial adoption: i) The issue of stability – the current record study maintains 95% of initial performance after approximately one year, which is significantly less than commercial silicon-module lifetimes of 20 – 30 years. Stability can be improved via several approaches such as composition engineering and optimization of the charge transporting layers (CTLs)[5]; ii) The challenge of toxicity – lead is incorporated in all of today's high efficiency perovskite solar cells. This is being tackled by several strategies, including lead recycling or device encapsulation[5]; iii) Unreliable scalability, which is the focus of this work. Scalable perovskite thin film deposition is a bottle neck to technological advancement.[5] While promising advances in device performance, reaching power conversion efficiencies (PCE) > 20%, were demonstrated with scalable fabrication methods, such as slot-die coating, spray coating, co-evaporation or blade coating,[6–9] performance losses with increasing device area are still substantial as compared to concurrent thin film PV technologies.[5] Consequently, manufacturing yield and reproducibility of large area perovskite PV are severe challenges.[10]

To maximize manufacturing yield, high quality in-line characterization is key. Using in-line characterization, the quality of thin films and device stacks can be assessed early in the fabrication process, reducing feedback cycle lengths for optimization and process monitoring.[11–15] In particular in-line

**ADVANCED
SCIENCE NEWS**

www.advancedsciencenews.com

**ADVANCED
MATERIALS
TECHNOLOGIES**

www.advmattechnol.de

photoluminescence (PL) measurements are widely employed[16,17] due to their non-invasive nature, simplicity and cost-effectiveness. The fundamental physics of PL are tied to the radiative or non-radiative recombination of photoexcited charge carriers.[18–23] Non-radiative recombination processes are promoted by bulk and surface defects,[22] including trap states, impurities, or structural defects. Radiative recombination occurs intrinsically as it is the inverse process of charge carrier excitation by light absorption from the valence band into the conduction band. Hence, a common assumption is that the higher the measured PL response of a semiconductor, the lower the non-radiative recombination and, in turn, the lower the defect density.[20] However, interpreting real PL measurements is much more complex, because PL intensity is also impacted by photon in- or out-coupling at film surfaces, as well as the interaction of light with optical components of individual setups.[24] A further drawback of conventional PL measurement of perovskites is potential inhomogeneities in the lateral perovskite thin film quality. A common error is to consider a PL measurement performed by single spot laser excitation as representative for the entire substrate without verifying homogeneity. This error may be neglectable for small substrates, but it is certainly not for large-scale solution-processed perovskite thin films.[25] Moreover, to unambiguously interpret a PL signal, a photoluminescence quantum yield (PLQY) analysis with an Ulbricht sphere is required that allows quantifying the total emitted number of photons.[21,24] Meanwhile, an accurate verification of the homogeneity can only be assured by a time-consuming scan over the sample. This results in long acquisition times, making the technique unsuitable for non-invasive in-line characterization.

Spatial imaging of the PL signal over the whole sample has been proposed as a strategy to address the issues of point-probe PL measurements.[25] In this context, Ternes et al. demonstrated large-scale PL imaging for in situ characterization of blade-coated perovskite thin films. Three different types of morphological defects were classified based on the comparison of their occurrence in different detection channels.[26] Despite these significant advances in analyzing perovskite homogeneity, a decisive PL quantity correlating with PLQY was not identified because of optically-induced artifacts varying across different PL setups. Dasgupta et al. proposed a solution to the problem of optical artifacts in PL intensity images by mapping the ideality factor n_{id}.[27] A common way to determine the ideality factor is to excite the sample with a laser in an integrating sphere and calculate the PLQY from the collected emitted light. The ideality factor can then be determined as described by Stolterfoht et al.,[28] Suchan et al.[29] and Thongprong et al.[30] Dasgupta et al. applied this methodology over the whole substrate area, starting from a spatially resolved PLQY map and utilizing a white reference for normalization.[27] While these results are promising, the white reference might be challenging to obtain in scalable coating setups.

In response, we present an alternative method based on the intensity dependent PL $\sim I_{in}^{k}$, with k being the power-law parameter and I_{in} the incident excitation intensity. We leverage the fact that the k-parameter serves as an accurate indicator of the relative magnitude of radiative and non-radiative recombination[31-34] – without the need of a PLQY map, nor a white reference for normalization. By varying intensities from 0.01 – 0.1 suns and collecting the corresponding PL response, we are able to directly determine a spatially resolved k-parameter. We demonstrate the robustness of this k-imaging method toward optically-induced artifacts as well as its ability to assign quality associations in terms of interfacial recombination when applied on different perovskite solar cell half stacks. The k-imaging method can facilitate the comparison of semiconductor quality between multiple fabrication batches at early stages, assisting with the decision of whether one batch of solar cells is worth completing, which makes it a very time-efficient tool. Altogether, the presented method is capable of a fast and spatially resolved quality assessment of large-area perovskite thin films, independent of optical film properties and PL setup geometry.

2. Results and Discussion

2.1. Methodology

In pursuit of finding an unambiguous and cost-effective characterization technique for perovskite thin film quality, we present a quantitative imaging technique based on intensity dependent photoluminescence. When sweeping excitation power, the intensity dependent PL signal follows a power-law with exponent k which is a potent quality indicator of the perovskite layer.[31] It was shown that the PL response relates to excitation intensity according to the following power-law:

$$I_{PL} \sim I_{in}^{k} \tag{1}$$

with k as the power-law parameter and I_{in} being the incident light intensity, where $k \in K$ with $K = \{x \in \mathbb{R} \mid 1 < x < 2\}$.[23] This relation can be explained by the PL rate equation as described by Schmidt et al.[31] This rate equation considers the two main recombination mechanisms, which are non-radiative Shockley-Read-Hall (SRH) recombination and bimolecular radiative recombination. We note that Auger recombination is neglectable in our setup, as we use sufficiently low excitation intensities.[35] In general, an increasing amount of crystal lattice imperfections, i.e., defects, leads to an increase of k toward 2.[23,31,33] With increasing excitation intensity, k is expected to approach the value 1, which represents pure radiative recombination. This is because the relative importance of trap-assisted non-radiative recombination declines as trap filling occurs. In summary, k = 1 indicates pure radiative recombination and k = 2 indicates dominant non-radiative recombination. Consequently, mechanisms potentially affecting the value of k include:

- interface recombination, in particular trap-assisted recombination,
- trap filling performance of the investigated sample,
- defects of any kind located within the sample.

The performance of a perovskite solar cell can be correlated with these processes,[36] which implies that the k-parameter is an indicator of perovskite thin film quality. A schematic of the core components of our k-imaging setup is shown in **Figure 1**. A scientific camera is employed for simultaneously imaging the entire sample. Two symmetrically aligned 467 nm LED bars homogeneously illuminate the underlying sample (see Figure 1a).
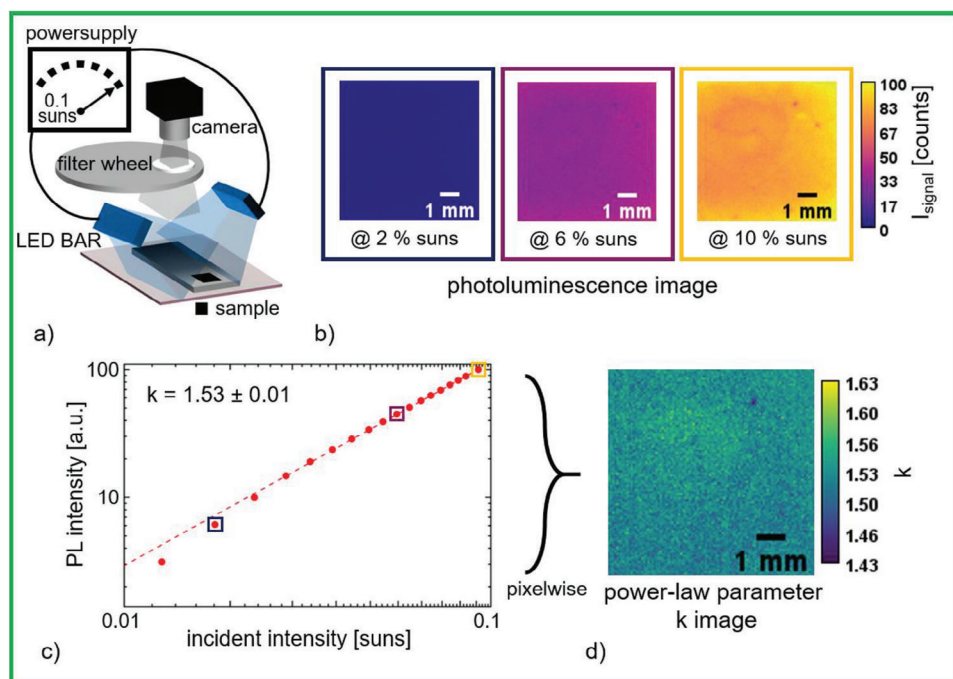
Figure 1. a) Experimental setup for determining the power-law parameter k on a test sample of size 7×7 mm^2 (black rectangle). The sample is placed under two symmetrically mounted 467 nm LED bars that ensure homogenous illumination (see Figure S1, Supporting Information) on a maximum detection area of (135×75) mm^2 (transparent bar). The emitted photoluminescence passes a 715 nm longpass filter and is captured by a sCMOS camera. b) Photoluminescence intensity image of the sample at different illumination intensities of 0.02 suns, 0.06 suns, and 0.1 suns c) PL intensity over the excitation intensity. PL intensities were calculated by average over the images shown in (b). A power-law fit leads to the power-law parameter $k = 1.53 \pm 0.01$. d) A similar fitting procedure as in (c) is carried out for each pixel (instead of the average intensity) resulting in the k image.

PL light passes through a filter blocking the excitation light before it is recorded by the camera. Images are acquired at 18 different intensities in the range of 0.01 – 0.1 suns in steps of 0.005 suns each (see Figure 1b). We determine k by fitting the mean PL of each image against the corresponding excitation intensity according to Equation 1, taking advantage of a log-log scale for better illustration purposes (see Figure 1c). After a background correction of the raw data the k-parameter can be fitted directly with Equation 1. Therefore, power-law analysis is optimal to accurately compare the quality of samples. The k-parameter can alternatively be determined for each pixel, resulting in an image with a spatial resolution of 70 μm per pixel (see Figure 1d). For this study, we place the camera at a distance of 25 cm from the sample which results in a k-image of 135×75 mm^2 (see Figure S1, Supporting Information).

Exposing the perovskite to light can enhance its quality by filling traps.[37] To prevent an artificial improvement in quality solely due to the experiment, we conducted a study where we systematically varied the duration of light soaking before measuring k-maps. As the duration of light soaking increased, the quality of the absorber improved, as evidenced by an increase in the k-parameter (see Figure S2, Supporting Information). To ensure consistent and comparable measurements, we maintained a standard light soaking time of 0 s for all samples. Enhanced pixel scales, adapted optics or multiple cameras would easily allow for examining m^2-area samples. Therefore, the presented k-imaging combines a high spatial resolution combined with a large detection window, making it capable of potential analysis for large-

scale perovskite solution processing. In addition, our technique is fast and bears potential for real-time quality control. The power-law parameter k image is determined in less than 5 min, with 1.5 min of acquisition time and 2.3 min of data analysis by a self-written software program, which ensures time-effective work. In future works, the data acquisition time can be decreased further by parallelizing the software code, allowing multiple processes to run simultaneously and high-speed data transfer.

2.2. Robustness

In this section we show that, unlike classical PL imaging, our k-imaging method is robust against PL artifacts and spatial variations of the setup optics. This robustness is crucial for the anticipated application of the methods for in-line metrology, since there is no standardized setup of a production line. Our home-built k-imaging method serves as a testbed to mimic different scenarios of these challenges.

2.2.1. Case I: Inhomogeneous Excitation

We first prove that the k-imaging method is robust toward inhomogeneous sample excitation. Photoluminescence of a semiconductor directly correlates to the excitation intensity. As a consequence, inhomogeneities in excitation due to stray light, reflections or inhomogeneous illumination lead to strong spatial
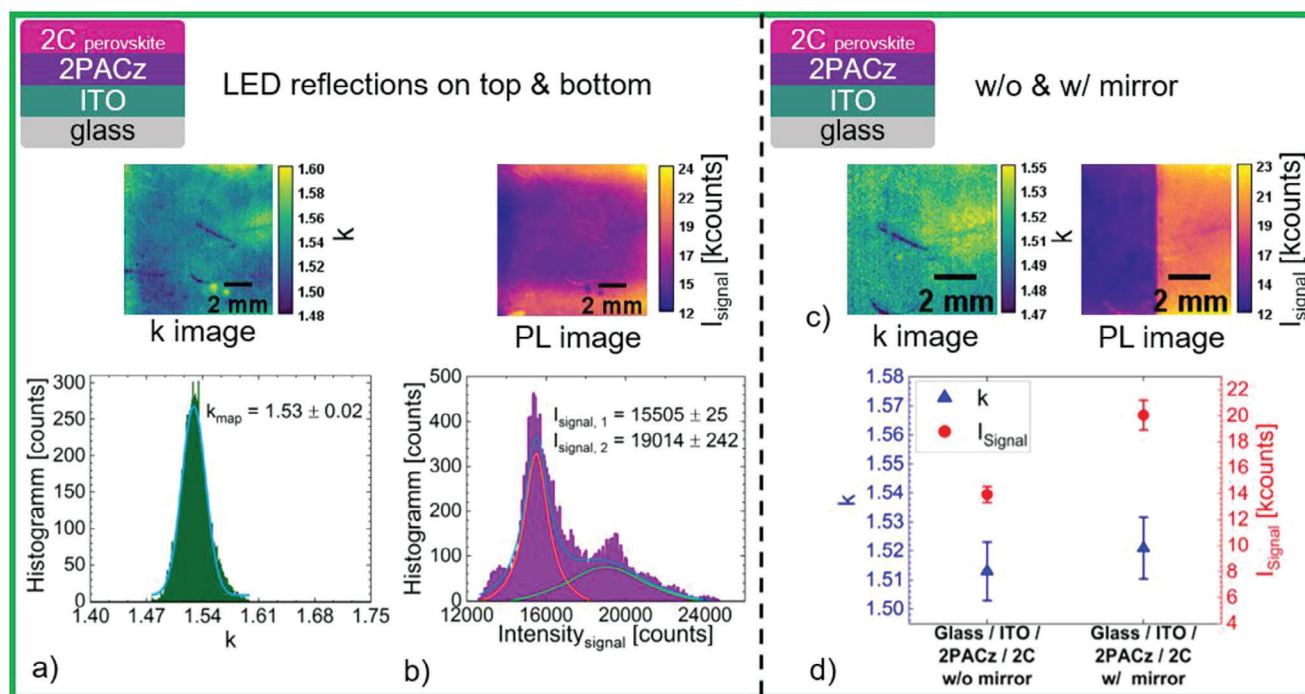
**ADVANCED
SCIENCE NEWS**

www.advancedsciencenews.com

**ADVANCED
MATERIALS
TECHNOLOGIES**

www.advmattechnol.de

Figure 2. a) k-image and k distribution of a glass / indium tin oxide (ITO) / (2-(9H-carbazol-9-yl) ethyl) phosphonic acid (2PACz) / double cation perovskite (2C) sample which is inhomogeneously illuminated. b) Corresponding PL image and PL distribution of a). c) Slope map and PL map of a sample covered with Glass / ITO / 2PACz / 2C which is positioned half on a mirror (left w/o, right w/). d) k and PL values of each area.

patterns in PL emission intensity. A representative example of inhomogeneous excitation is shown in **Figure 2**a,b. While qualitative analysis remains feasible to a certain extent, quantification of the homogeneity and intensity of PL emission for such a setup is very inaccurate. In contrast, although the top and bottom regions of the sample experience a much higher excitation leading to a much higher PL signal (23 ± 1) %, the k-image remains uniform over the entire substrate (see Figure 2a,b). Hence, we conclude that only the intensity dependent PL carries all required information to accurately disentangle the information on the quality of the perovskite thin film from the excitation intensity. In summary, a prominent advantage of the k-imaging method is its robustness to inhomogeneity-induced artifacts, making the obtained results highly comparable to those from other setups.

2.2.2. Case II: Reflective Stages or Substrates

Next, we demonstrate that our k-imaging method is also robust toward variations in emission characteristics of the thin film or operational environment. In detail, we show that k-images are robust in the presence of variations in reflectivity underneath the investigated sample, which mimics spatial variations in the optical response of the setup or variations in the PL outcoupling from the sample. We examine a sample positioned in a way that half of its surface is placed over a mirror. Although the perovskite layer itself is very homogeneous, a (44 ± 10) % enhanced PL signal is found in the region over the mirror, while the power-law parameter k stays constant (see Figure 2c,d). Thus, the intensity of the PL signal is not a reliable quality indicator of the perovskite

film because it is sensitive to slight variations of the optical film properties. In contrast, the k-image provides a homogeneous response, manifesting that the information derived from the intensity dependent PL is robust toward relative spatial variations in PL outcoupling or variations in the optics of the setup.

This robustness toward experimental PL artifacts makes the k-imaging method superior to common PL mapping. Consequently, the method is an ideal candidate for in-line applications such as a control unit that monitors the manufacturing process of large-scale substrates.

2.3. Validation

In the following, we establish the accuracy and reliability of the method. To benchmark the k parameter as a decisive indicator for perovskite thin film quality, we compare the k-imaging method with a reference state-of-the-art PLQY measurement recorded in an integrating sphere.

We compare three different half stacks to investigate the effect of certain hole transport layers (HTLs) on interfacial recombination. Glass / indium tin oxide (ITO) / triple cation perovskite (3C) are used as a HTL-free reference, while one sample has (2-(9H-carbazol-9-yl) ethyl) phosphonic acid (2PACz) as HTL and the other has a spin-coated nickel oxide (NiO_x) and 2PACz bilayer (see **Figure 3**a–c). We perform PL measurements at varied intensities from 0.06 to 2 suns with a 515 nm laser in an integrating sphere (see Figure 3d). The samples are excited in the center and PL is collected from all sides. Remarkably, results obtained from our k-imaging method show the same trend as those from the
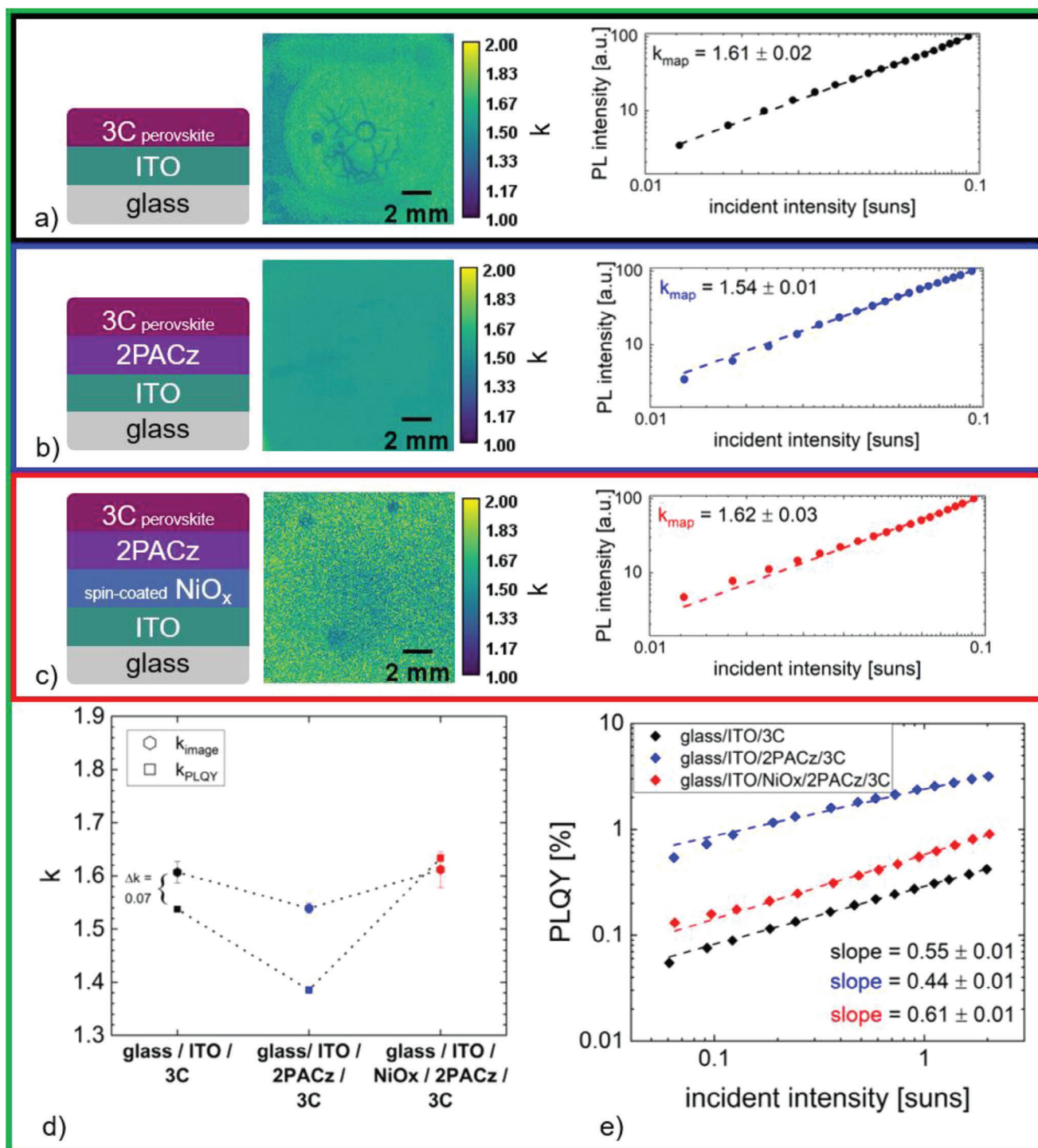
Figure 3. a–c) k images and plots highlighting the mean k data of different half stacks: glass / ITO / 3C, glass / ITO / 2PACz / 3C, Glass / ITO / NiO$_x$ / 2PACz / 3C with spin coated HTL layers. d) Comparison of the power-law factor k determined by measurements of the presented setup and within an integrated sphere. e) PLQY versus I$_{in}$ results of the different half stacks.

benchmark state-of-the-art method which confirm the validity of our method (see Figure 3d). Due to the intensity dependence of the k-parameter we expect it to be lower in the benchmark experiment where the laser excitation intensity is a bit higher and, thus, more trap states are expected to be filled. We can confirm this ex-

pectation for the glass / ITO / 3C half stack where the k$_{PLQY}$ value is 0.07 lower compared to k$_{image}$. Similarly, in the glass / ITO / 2PACz / 3C half stack, there is a reduced k$_{PLQY}$ value, precisely by 0.15 (Figure 3d). The k-parameter of the glass / ITO / NiOx / 2PACz / 3C half stack is roughly equivalent for both methods

ADVANCED
SCIENCE NEWS

www.advancedsciencenews.com

ADVANCED
MATERIALS
TECHNOLOGIES

www.advmattechnol.de

(see Figure 3d), indicating that k exhibits no strong intensity dependence within the range of 0.01 – 2 suns. Looking at Figure 3e, it becomes evident that its PLQY curve exhibits no trend toward saturation at higher intensities and has the highest slope. We attribute this to a higher magnitude of trap assisted non-radiative recombination in the samples with NiOx as compared to the ones without (see further discussion below).[38]

By taking advantage of the imaging capabilities of our method, we can identify not only pinholes, but also a ring of varying k-values originating from the anti-solvent step used in our particular spin coating process (see Figure 3a). The anti-solvent ring shows an increased k as compared to the rest of the sample. This observation suggests that non-radiative recombination is enhanced by an imperfect morphology and the crystallization of the perovskite is impeded if the precursor solution is far from supersaturation. This situation occurs when antisolvent is dripped too early, resulting in a wet film that remains too thick.[39] Another possibility for the emergence of the ring can be the vacuum suction that holds the sample in place altering local temperature, impacting crystallization dynamics.

Subsequently, we investigate the consistency of our results according to literature. Al-Ashouri et al. report that the self-assembled-monolayer (SAM) 2PACz not only covers rough surfaces conformally but also creates an energetically beneficial interface with the perovskite layer which leads to minimal non-radiative recombination.[40] Consequently, we expect the lowest k to be observed with the stack employing 2PACz and indeed our result confirms this theory (see Figure 3d). However, a defect-free coverage of 2PACz highly depends on pre-treatment of the ITO interface.[41,42] To decouple the device operation from the ITO pre-treatment, NiOx is suggested to be added as an interlayer between the anode and HTL by spin coating. Unfortunately, this creates small surface defects as 2PACz reacts with the oxygen of NiOx, which benefits non-radiative recombination processes.[43] Thus, we expect an increase of k for the NiOx containing stack, which is confirmed as shown in Figure 3.

In summary, the k-images shown in Figure 3a–c follow the same trend in magnitude as expected consistently over the entire substrate, but also reveal pinholes and inhomogeneities that can be correlated with the antisolvent step. This level of detail highlights the strength of our k-imaging method.

2.4. Applications of the k-Imaging Method

2.4.1. Determining Interfacial Quality Through Imaging Various Potential Layer Combinations on a Single Substrate

The k-imaging method can also be applied to identify variations in film quality and device architecture. In the following, the effectiveness of k-image analysis is examined by comparing the k-parameter map of four different architectures processed on a single substrate by varying the underlying perovskite/HTL interface. The four half stacks are: area 1: glass / ITO / 2PACz / double cation perovskite (2C), area 2: glass / ITO / NiOx / 2PACz / 2C, area 3: glass / 2PACz / 2C, and area 4: glass / NiOx / 2PACz / 2C (see **Figure 4**a). We observe significant variations of the k-parameter for the four areas. It ranges from $k_{area\ 3} = 1.33 \pm 0.01$ to $k_{area\ 1} = 1.52 \pm 0.03$.

The investigation of different layer sequences (see Figure 4b) offers i) the opportunity to identify the origin of a defect within the layer stack and ii) it allows drawing conclusions about the impact of certain layers on interfacial recombination. Figure 4b illustrates the differences in k between all areas. As a first step we investigate the impact of ITO by comparing area 1 to 3 followed by a comparison of area 2 to 4. The parameter $k_{area\ 1} = 1.52 \pm 0.03$ is enhanced compared to $k_{area\ 3} = 1.33 \pm 0.01$, which implies that the non-radiative recombination increases. We attribute this to an increased grain size of the perovskite layer as 2PACz adheres directly to glass in the absence of the anode (Figure S5, Supporting Information). An increased grain size leads to higher radiative recombination as previously observed by Watthage et al.[44] Furthermore, the ITO layer facilitates charge transport in a manner that benefits the non-radiative channel, indicated by the nine times lower PL signal of the area 1 stack (Figure 4c).

A comparison of the k-parameter of area 2 and area 4 shows that both are similar with $k_{area\ 2} = 1.38 \pm 0.05$ and $k_{area\ 4} = 1.39 \pm 0.05$, respectively. The difference of area 2 and 4 as compared to area 1 and 3 is the NiOx layer. Therefore, we investigate the impact of NiOx by comparing area 3 to 4 and area 1 to 2. The presence of sputtered NiOx decreases the impact of the anode on interfacial recombination because the NiOx /2PACz interface is now the most influential. Consistently, the layer sequence from the NiOx layer onwards is identical for both stacks and both SEM images look similar, implying that crystallization and grain size of the perovskite layer is comparable (Figure S5, Supporting Information). Furthermore, the PL intensity is similarly low for both stacks (Figure 4c). Therefore, the layer sequence until NiOx has a neglectable contribution. This can be explained by the effect where addition of NiOx decreases the PL, which was previously observed by Du et al.[45] According to their assumption, this is due to enhanced hole extraction, which leads to lower radiative recombination. Therefore, we expect an increased k if NiOx is added. Indeed, this is the case when comparing $k_{area\ 3} = 1.33 \pm 0.01$ without NiOx to $k_{area\ 4} = 1.39 \pm 0.05$ with NiOx, confirming their assumption. The same trend is apparent in the previous comparison of glass / ITO / 2PACz / 3C to glass / ITO / NiOx / 2PACz / 3C (see again Figure 3d). However, by comparing $k_{area\ 1} = 1.52 \pm 0.03$ without NiOx to $k_{area\ 2} = 1.38 \pm 0.05$ with NiOx, the opposite effect is visible. We attribute this to the different deposition techniques. For this study ITO and NiOx were sputtered, while the NiOx in Figure 3c was spin coated. A comparison to the lifetimes of each stack validates the trend observed in the k-parameters (see Figure S9, Supporting Information).

Lastly, we discuss the variations in full width half maximum (FWHM) apparent for the k-parameter distribution in the four areas. The FWHM values remain sufficiently low for a meaningful analysis with a maximum of 0.12 for the area 4 stack. Likewise, even the lowest signal to noise ratio (S/N) which is delivered by the area 2 stack is sufficiently high at 2.7 ± 0.3 (Figure S10, Supporting Information) holding the minimal threshold of S/N = 3 for achieving true signals.[46]

In summary, we show that the k-imaging method is a powerful tool to identify and analyze spatial variations in device architectures. The method is sufficiently sensitive to identify pinholes, partly incomplete interlayer depositions or any other variation in the device architecture which might result from imperfect
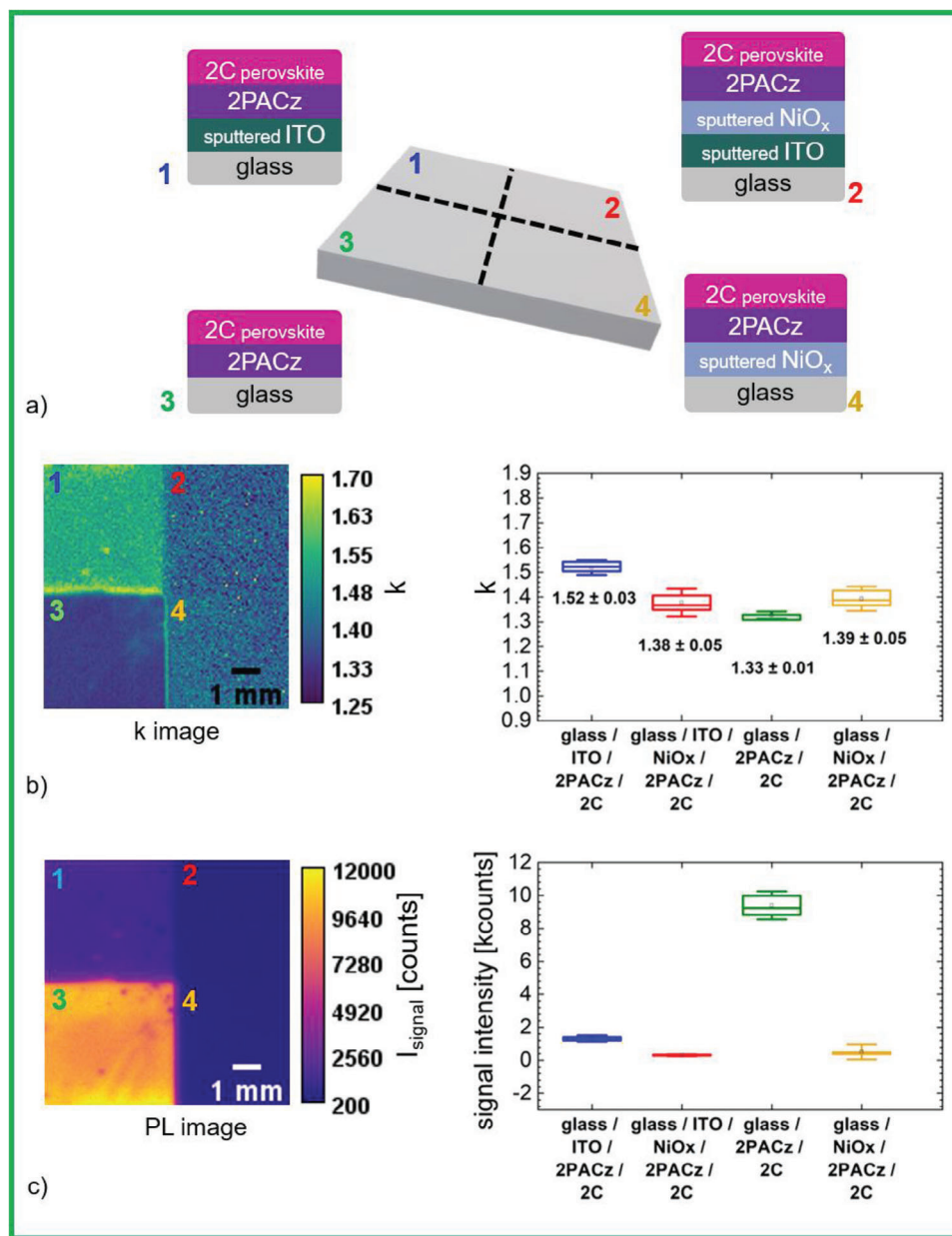
**ADVANCED
SCIENCE NEWS**

www.advancedsciencenews.com

**ADVANCED
MATERIALS
TECHNOLOGIES**

www.advmattechnol.de

Figure 4. a) Sketch of a sample coated with different half stacks within one sample. Area 1: glass / ITO / 2PACz / 2C. Area 2: glass / ITO / NiO$_x$ / 2PACz / 2C. Area 3: glass / 2PACz / 2C. Area 4: glass / NiO$_x$ / 2PACz / 2C. b) Slope maps and k values of the different regions. c) Corresponding PL map and values of (b).

processing. Moreover, the k-parameter analysis allows us to correlate variations in device architecture to changes in interfacial recombination.

2.4.2. Passivation Concentration Optimization and Correlation to Open-Circuit Voltage V_{OC}

Finally, we demonstrate that the k-imaging method is sufficiently sensitive to distinguish fine variations of perovskite thin film quality that correlate with changes in perovskite solar cell performance, particularly in open-circuit voltage (V_{OC}) with steps of

20 mV. For this, we compare different bulk passivation concentrations with each other as these are expected to affect the V_{OC} of the test devices.

Phenethyl ammonium iodide (PEAI) has recently been shown to be an effective surface passivation layer.[47] Therefore, it is good candidate for testing the versatility of k-imaging in investigating semiconductor modification techniques. In detail, we test the correlation of the k-parameter and perovskite solar cell device performance with PEAI concentration as a bulk passivant. A widely established route to realize high quality passivation of perovskite thin films is processing multiple batches of solar cells with varying passivation concentrations. These solar cells are tested for
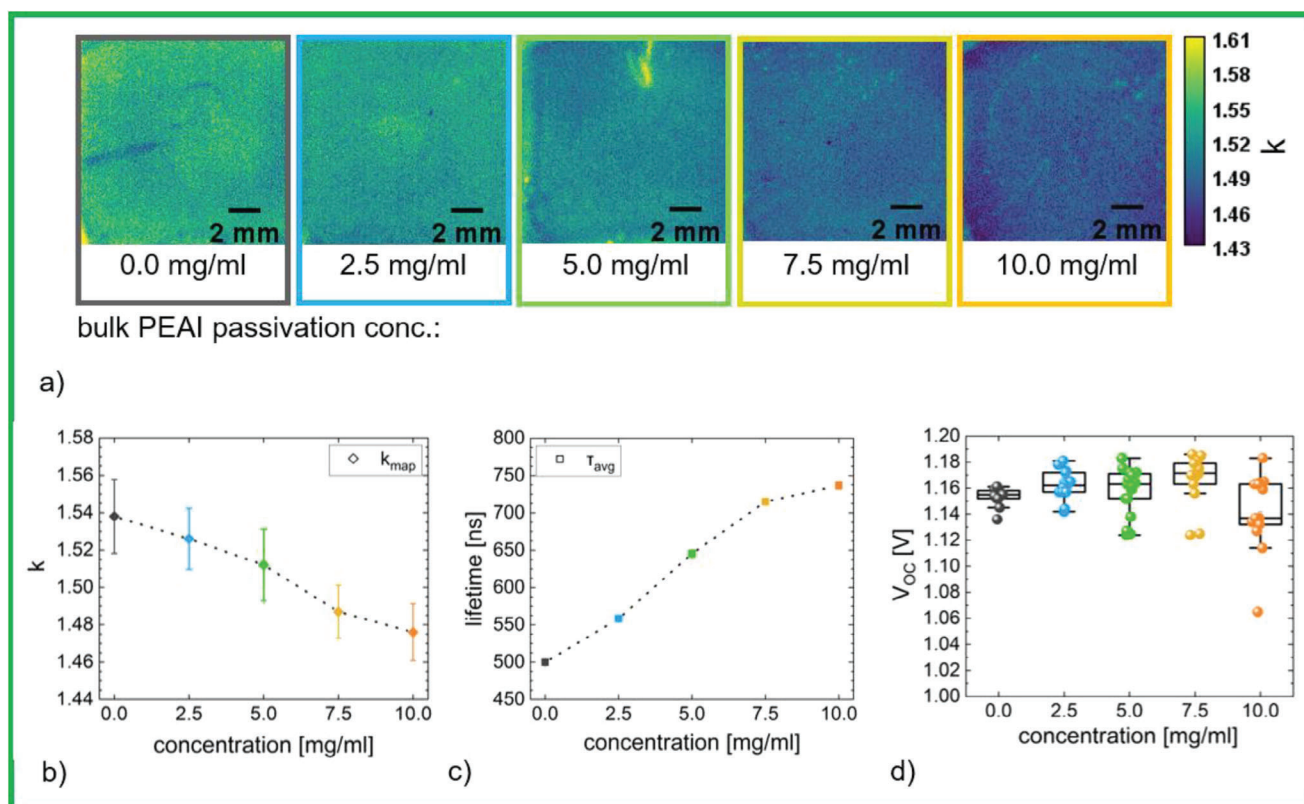
**ADVANCED
SCIENCE NEWS**

www.advancedsciencenews.com

**ADVANCED
MATERIALS
TECHNOLOGIES**

www.advmattechnol.de

Figure 5. a) Slope maps of samples covered with glass / ITO / 2PACz / 3C (incl. varying PEAI concentrations from 0.0 to 10.0 mg ml^{-1}. b) Trend of k dependent on passivation concentration. c) Lifetimes for each passivation concentration. d) V_{OC} variation with passivation concentration.

their electrical properties and the concentration with the best performance is selected as optimal. To demonstrate the correlation of all mentioned parameters we apply the k-imaging method. A glass / ITO / 2PACz / 3C stack is analysed with PEAI concentrations ranging from 0 – 10 mg ml^{-1} in 2.5 mg ml^{-1} increments (see **Figure 5**a). To ensure statistical relevance, each datapoint in Figure 5b represents the mean value of the corresponding image in Figure 5a consisting of 180 × 180 pixels.

Figure 5b shows that with increasing bulk PEAI concentration the k-parameter decreases and that no defects or clusters were formed, indicating enhanced perovskite film quality. Further validation of this indication is provided by time-resolved photoluminescence (TRPL) measurements, which yield the lifetime of the absorber. A longer lifetime signifies a higher layer quality.[37] Consequently, the k-parameter exhibits an inverse trend to the lifetime (see Figure 5b,c; Figure S11, Supporting Information). A comparison of the k-parameter to device V_{OC} confirms an improvement in V_{OC} toward higher PEAI concentrations (see Figure 5d). The sensitivity of k-parameter analysis is demonstrated by its ability to distinguish differences in 20 mV steps of the V_{OC}. However, 7.5 mg ml^{-1} PEAI with a V_{OC} of (1.17 ± 0.02) V and a PCE of (16.99 ± 1.35) % (see Figure S4, Supporting Information) is identified as the optimal concentration whereas the best k-parameter is found for 10 mg ml^{-1}. We attribute the deviation of optimal concentration to the fact that the k-parameter is determined by investigating a half stack which specifically provides information on the recombination processes. In contrast,

the PCE is also affected by reduced charge extraction that might result in higher series resistance (R_s) and thus a reduced fill factor. In that regard, Ansari et al. and Gharibzadeh et al. showed that a higher passivation concentration can result in an increased R_s which decreases the fill factor (see Figure S4, Supporting Information).[48,49] In addition, completion of a full device requires additional fabrication steps which increases the probability of fabrication errors.

Concluding, while k-parameter analysis and the full perovskite solar cell device PCE deliver slightly different optimal concentrations, the correlation of the k-parameter to passivation concentration offers the opportunity to use the k-imaging method as a control unit to monitor the effectiveness and homogeneity of passivation molecules. As bulk passivation sensitively affects V_{OC} it is of crucial importance to identify deviant areas during the industrial fabrication of a large-scale device. Ranges may be set in which the k-parameter is allowed to remain and consequently, well-founded decisions can be made of whether or not a particular batch is to be finished.

3. Conclusion and Outlook

This work presents a robust, non-invasive and high-resolution imaging method for assessment of perovskite thin film quality. The method is fast and scalable, making it a potent candidate for in-line quality control of large-scale perovskite PV processing. It relies on measurements of the intensity dependent PL that

**ADVANCED
SCIENCE NEWS**

www.advancedsciencenews.com

**ADVANCED
MATERIALS
TECHNOLOGIES**

www.advmattechnol.de

follows a power-law with exponent k which is a decisive indicator of the perovskite layer quality regarding radiative and non-radiative recombination.

The presented k-imaging method is shown to reveal information on layer quality even in the presence of stray light, reflections and similar optical artifacts originating from the setup. The spatial resolution also reveals information about homogeneity of the absorption layer in terms of pinholes or other defects. Furthermore, the k-imaging method gives valuable insights into the interfacial recombination quality of any layer sequence. In addition, this method shows the advantage of correlating the k-parameter with bulk passivation concentration. This correlation allows this method to not only serve as a control unit for monitoring passivation layer homogeneity but also for predicting device V_{OC} in a 20 mV range as it is very sensitive to bulk passivation. Boundaries for k can be set and the k-value monitored to lie within these boundaries, ensuring a successful passivation. This eases the decision whether a batch should be completed and consequently the k-imaging method can be used as an in-line application at any stage of the fabrication process. Furthermore, our method enables in situ investigations, as demonstrated in Figure S12 (Supporting Information), confirming its utility for studying degradation processes. This capability opens up opportunities for further in situ research aimed at enhancing layer quality, such as vapor passivation,[50] and contributing to the optimization of various processes. In-line characterization methods ask for a compact setup architecture and fast determination of the requested parameter. The k-imaging method fits these requirements as only a camera, filter and light sources are needed. The current data acquisition time takes 1.5 min and the analysis 2.3 min. Further optimization of the software program and high-speed data transfer will enable a real-time quality control unit. In conclusion, the presented k-imaging method proves to be versatilely applicable not only for large-scale perovskite solution processing, but also for scientific investigations of interfacial recombination and passivation homogeneity.

4. Experimental Section

Sample Preparation: *Substrates and HTL*: ITO substrates (sheet resistance 15 Ω sq^{-1}, Luminescence Technology, CAS: 50926-11-9) were cut to 0.16 cm × 0.16 cm and cleaned with acetone and isopropanol in an ultrasonic bath for 10 min each. Substrates were further treated with oxygen plasma for 3 min before spin-coating a 2PACz hole transport layer at 3000 rpm for 30 s and subsequently annealed at 100 °C for 10 min. The 2PACz precursor solution was prepared by dissolving 2PACz in anhydrous ethanol with a concentration of 1 mM and before usage it was placed in an ultrasonic bath for at least 30 min.

Perovskite Solution: The double cation perovskite solution with the stoichiometric formula $FA_{0.83}Cs_{0.17}Pb(I_{0.92}Br_{0.08})_3$ was prepared by dissolving PbI_2 (TCI, 444 mg), $PbBr_2$ (TCI, 46 mg), CsI (ABCR, 46 mg), and FAI (Greatcell, 143 mg) in 1 ml DMF:DMSO (4:1 volume ratio).

The triple cation perovskite solution was prepared by mixing PbI_2 (1.21 M), $PbBr_2$ (0.37 M), CsI (0.075 M), MABr (0.34 M), and FAI (1.11 M) in a mixture of DMF:DMSO (4:1 v/v) resulting in a composition described by $Cs_{0.05}(FA_{0.77}MA_{0.23})_{0.95}Pb(I_{0.77}Br_{0.23})_3$ and a thin film with a bandgap of 1.68 eV when spin-coated. For preparing the bulk passivation (BP) perovskite solution, stock solutions of phenethyl ammonium iodide (PEAI) dissolved in DMF:DMSO (4:1) with different concentrations (2.5, 5, 7.5, and 10 mg ml^{-1}) were prepared. Then the solution was added in the reference perovskite solution with a molar ratio of 1:19.

Perovskite Film Fabrication: The double cation perovskite was deposited by spin-coating at 1000 rpm (acceleration 2000 rpms^{-1}) for 10 s and 5000 rpm (acceleration 2000 rpms^{-1}) for 40 s. Twenty seconds after the start of the second spin-coating step, the spinning substrate was washed with 150 µl chlorobenzene. The perovskite film was subsequently annealed at 100 °C for 30 min on a preheated hotplate in an inert atmosphere.

The triple cation perovskite films were spin-coated on substrates at 1000 rpm (200 rpm s^{-1}) for 10 s and 5000 rpm (2000 rpm s^{-1}) for 30 s. 15 – 20 s after the start of the second step, ethyl acetate (150 µL) was casted at the center of the spinning substrate. The samples were then annealed at 100 °C for 30 min in a nitrogen atmosphere.

Triple Cation Solar Cell: The planar p-i-n perovskite solar cells were fabricated with the architecture of: glass / ITO / 2PACz / $Cs_{0.05}(FA_{0.77}MA_{0.23})_{0.95}Pb(I_{0.77}Br_{0.23})_3$ / LiF / C_{60} / BCP / Ag. After the deposition of the perovskite thin film, a 1-nm layer of LiF followed by 23 nm of C_{60} and 3 nm BCP as the electron transport layer (ETL) were sequentially evaporated by thermal processes at a rate of 0.1 – 0.2 A/s while maintaining a pressure not higher than 10^{-6} mbar. Finally, a 100-nm layer of Ag was thermally evaporated using a shadow mask with an active area of 10.5 mm^2 to complete the perovskite solar cells with 4 pixels per substrate.

Sputter System: (ITO, 135 nm) was sputtered using a Kurt J. Lesker PVD-75 thin film deposition system from a target (In_2O_3:SnO_2 90:10, Kurt J. Lesker). A power of 50 W and a gas composition of 97.5% Ar to 2.5% O2 at a pressure of 0.8 mTorr was used for 2200 s. The sheet resistance of the ITO film is ≈27 Ω cm^{-2}. NiO_x (15 nm) was sputtered at room temperature with a power of 100 W from a NiO_x target (99.9% Kurt J. Lesker) with pure Ar at 1 mTorr for 450 s. The composition was stoichiometric which was confirmed by X-ray photoelectron spectroscopy (XPS) and X-ray diffraction (XRD) data (Figure S13, Supporting Information). For the preparation of 4 different half stacks within one sample first ITO was sputtered covering half of the glass substrate by using a half mask and afterward a new half mask was positioned perpendicular to the first one to sputter NiO_x.

Characterization Techniques: *Power-Law Parameter k Mapping*: Two 467 nm LED bars (LDL2-170/30-BL2, Creating Customer Satisfation Inc., Puchheim-Germany) were symmetrically aligned to homogeneously illuminate the underlying sample. (see Figure S1, Supporting Information). The resulting PL signal was recorded by a sCMOS camera (CS2100M-USB – Quantalux 2.1 MP Monochrome sCMOS Camera, Thorlabs, Bergkirchen-Germany). The maximal detection window of the setup was (135 × 75) mm^2 (see Figure S1, Supporting Information). The camera was positioned 25 cm from the sample. The excitation light was filtered by a 715 nm longpass filter (50.8 mm, SQ 715 nm, LongPass Color Filter, Thorlabs, Bergkirchen-Germany) positioned directly in front of the camera (see Figure 1a). Images were acquired at 18 different intensities in the range of 0.01 – 0.1 suns in 0.005 sun steps. It was ensured that only the PL was recorded by performing a background correction. The symmetrical alignment of the LEDs guarantees a homogeneous illumination of the sample and therefore inhomogeneities within the k images were not due to the excitation source (see Figure S1, Supporting Information). The k-parameter was directly determined for each pixel by plotting the PL signal toward the corresponding excitation intensity I_{in} and then fitting it by $PL = Const \cdot I_{in}^k$.

Scanning Electron Microscopy (SEM): Field emission top-view scanning electron microscopy (SEM) images of perovskite layers were taken with a ZEISS Supra60 VP scanning electron microscope.

Photoluminescence Quantum Yield (PLQY): PLQY measurements were performed inside an integrating sphere (LabSphere, 15 cm diameter) in ambient air (relative humidity <30%). A 515 nm laser (LD-515-10MG from Roithner Lasertechnik) was directed into the sphere via a small entrance port. An optical fiber collected the emission from the exit port and was directed to the spectrometers (QE65 Pro from Ocean Optics from Avantes). The spectral response was calibrated using a calibration lamp (HL-3plus-INT-Cal from Ocean Optics). Raw measured spectra were recalculated to give power spectra using the integration time. PLQY was determined by following the method described by de Mello et al.[51] The samples were placed at an angle of 15° with respect to the laser beam to avoid specular reflectance toward the entrance port.

**ADVANCED
SCIENCE NEWS**

www.advancedsciencenews.com

**ADVANCED
MATERIALS
TECHNOLOGIES**

www.advmattechnol.de

Time-Correlated Single Photon Counting (TCSPC): TCSPC measurements were performed with a FLS920 fluorescence spectrometer (Edinburgh Instruments Ltd 2006). A 635 nm laser (LDH-P-635, PicoQuant) was directed to the sample at 50 kHz repetition rate. The initial density was $3.0 \cdot 10^{14}$ cm^{-3}.

Supporting Information

Supporting Information is available from the Wiley Online Library or from the author.

Acknowledgements

Conflict of Interest

The authors declare no conflict of interest.

Data Availability Statement

The data that support the findings of this study are available from the corresponding author upon reasonable request.

Keywords

[1] N. M. Haegel, R. Margolis, T. Buonassisi, D. Feldman, A. Froitzheim, R. Garabedian, M. Green, S. Glunz, H. M. Henning, B. Holder, I. Kaizuka, B. Kroposki, K. Matsubara, S. Niki, K. Sakurai, R. A. Schindler, W. Tumas, E. R. Weber, G. Wilson, M. Woodhouse, S. Kurtz, *Science* **2017**, *356*, 141.

[2] N. G. Park, K. Zhu, *Nat. Rev. Mater.* **2020**, *5*, 333.

[3] Z. Li, T. R. Klein, D. H. Kim, M. Yang, J. J. Berry, M. F. A. M. van Hest, K. Zhu, *Nat. Rev. Mater.* **2018**, *3*, 18017.

[4] E. L. Unger, L. Kegelmann, K. Suchan, D. Sörell, L. Korte, S. Albrecht, *J. Mater. Chem. A* **2017**, *5*, 11401.

[5] S. Ternes, *In situ characterization and modelling of drying dynamics for scaleable printing of hybrid perovskite photovoltaics,* KIT Scientific Publishing, Karlsruhe, Germany **2023**.

[6] J. Li, J. Dagar, O. Shargaieva, M. A. Flatken, H. Köbler, M. Fenske, C. Schultz, B. Stegemann, J. Just, D. M. Többens, A. Abate, R. Munir, E. Unger, *Adv. Energy Mater.* **2021**, *11*, 2003460.

[7] H. Cai, X. Liang, X. Ye, J. Su, J. Guan, J. Yang, Y. Liu, X. Zhou, R. Han, J. Ni, J. Li, J. Zhang, *ACS Appl. Energy Mater.* **2020**, *3*, 9696.

[8] J. Li, H. Wang, X. Y. Chin, H. A. Dewi, K. Vergeer, T. W. Goh, J. W. M. Lim, J. H. Lew, K. P. Loh, C. Soci, T. C. Sum, H. J. Bolink, N. Mathews, S. Mhaisalkar, A. Bruno, *Joule* **2020**, *4*, 1035.

[9] S. Chen, X. Dai, S. Xu, H. Jiao, L. Zhao, J. Huang, *Science* **2021**, *373*, 902.

[10] X. Niu, N. Li, Q. Chen, H. Zhou, *Adv. Energy Sustainability Res.* **2021**, *2*, 2000046.

[11] F. Laufer, S. Ziegler, F. Schackmar, E. A. Moreno Viteri, M. Götz, C. Debus, F. Isensee, U. W. Paetzold, *Sol. RRL* **2023**, *7*, 2201114.

[12] M. Z. Rahman, T. Edvinsson, *Chapter 2 – X-ray diffraction and raman spectroscopy for lead halide perovskites, Characterization Techniques for Perovskite Solar Cell Materials, In Micro and Nano Technologies,* Elsevier, Amsterdam **2020**, pp. 23–47.

[13] M. Abdi-Jalebi, M. Ibrahim Dar, A. Sadhanala, E. M. J. Johansson, M. Pazoki, *Chapter 3 – Optical absorption and photoluminescence spectroscopy, In Micro and Nano Technologies, Characterization Techniques for Perovskite Solar Cell Materials,* Elsevier, Amsterdam **2020**, pp. 49–79.

[14] M. Pazoki, T. Edvinsson, *Chapter 6 – Time resolved photo-induced optical spectroscopy, In Micro and Nano Technologies, Characterization Techniques for Perovskite Solar Cell Materials,* Elsevier, Amsterdam **2020**, pp. 139–160.

[15] S. Ternes, T. Börnhorst, J. A. Schwenzer, I. M. Hossain, T. Abzieher, W. Mehlmann, U. Lemmer, P. Scharfer, W. Schabel, B. S. Richards, U. W. Paetzold, *Adv. Energy Mater.* **2019**, *9*, 1901581.

[16] S. Siebentritt, T. P. Weiss, M. Sood, M. H. Wolter, A. Lomuscio, O. Ramirez, *J. Phys. Mater.* **2021**, *4*, 042010.

[17] A. D. Bui, M. A. Mahmud, N. Mozaffari, R. Basnet, T. Duong, G. Bartholazzi, T. T. Le, T. N. Truong, M. Tebyetekerwa, A. Wibowo, K. J. Weber, T. P. White, K. R. Catchpole, D. Macdonald, H. T. Nguyen, *Sol. RRL* **2021**, *5*, 2100348.

[18] Q. Zhou, B. Wang, R. Meng, J. Zhou, S. Xie, X. Zhang, J. Wang, S. Yue, B. Qin, H. Zhou, Y. Zhang, *Adv. Funct. Mater.* **2020**, *30*, 2000550.

[19] J. Chen, C. Zhang, X. Liu, L. Peng, J. Lin, X. Chen, *Photon. Res.* **2021**, *9*, 151.

[20] T. Kirchartz, J. A. Márquez, M. Stolterfoht, T. Unold, *Adv. Energy Mater.* **2020**, *10*, 1904134.

[21] I. Pelant, J. Valenta, *Luminescence Spectroscopy of Semiconductors,* Oxford Univ. Press, Oxford **2012**.

[22] H. Cheng, Y. Feng, Y. Fu, Y. Zheng, Y. Shao, Y. Bai, *J. Mater. Chem. C* **2022**, *10*, 13590.

[23] H. Shibata, M. Sakai, A. Yamada, K. Matsubara, K. Sakurai, H. Tampo, S. Ishizuka, K. K. Kim, S. Niki, *Jpn. J. Appl. Phys.* **2005**, *44*, 6113.

[24] P. Fassl, V. Lami, F. J. Berger, L. M. Falk, J. Zaumseil, B. S. Richards, I. A. Howard, Y. Vaynzof, U. W. Paetzold, *Matter* **2021**, *4*, 1391.

[25] J. Hidalgo, A. Castro-Méndez, J. Correa-Baena, *Adv. Energy Mater.* **2019**, *9*, 1900444.

[26] S. Ternes, F. Laufer, P. Scharfer, W. Schabel, B. S. Richards, I. A. Howard, U. W. Paetzold, *Sol. RRL* **2022**, *6*, 2100353.

[27] A. Dasgupta, S. Mahesh, P. Caprioglio, Y. H. Lin, K. A. Zaininger, R. D. J. Oliver, P. Holzhey, S. Zhou, M. M. McCarthy, J. A. Smith, M. Frenzel, M. G. Christoforo, J. M. Ball, B. Wenger, H. J. Snaith, *ACS Energy Lett.* **2022**, *7*, 2311.

[28] M. Stolterfoht, M. Grischek, P. Caprioglio, C. M. Wolff, E. Gutierrez-Partida, F. Peña-Camargo, D. Rothhardt, S. Zhang, M. Raoufi, J. Wolansky, M. Abdi-Jalebi, S. D. Stranks, S. Albrecht, T. Kirchartz, D. Neher, *Adv. Mater.* **2020**, *32*, 2000080.

[29] K. Suchan, J. Just, P. Becker, E. L. Unger, T. Unold, *Mater. Chem. A* **2020**, *8*, 10439.

[30] N. Thongprong, T. Supasai, Y. Li, I. Tang, N. Rujisamphan, *Energy Technol.* **2020**, *8*, 1901196.

[31] T. Schmidt, K. Lischka, W. Zulehner, *Phys. Rev. B* **1992**, *54*, 8989.

[32] C. Spindler, T. Galvani, L. Wirtz, G. Rey, S. Siebentritt, *J. Appl. Phys.* **2019**, *126*, 175703.

[33] T. Schmidt, G. Daniel, K. Lischka, *J. Cryst. Growth* **1992**, *117*, 748.

[34] F. Babbe, L. Choubrac, S. Siebentritt, *Sol. RRL* **2018**, *2*, 1800248.

[35] D. W. deQuilettes, K. Frohna, D. Emin, T. Kirchartz, V. Bulovic, D. S. Ginger, S. D. Stranks, *Chem. Rev.* **2019**, *119*, 11007.

[36] T. Kirchartz, U. Rau, *Adv. Energy Mater.* **2018**, *8*, 1703385.

[37] L. Lin, L. Yang, G. Du, X. Li, J. Deng, K. Wei, J. Zhang, *ACS Appl. Energy Mater.* **2023**, *6*, 10303.

[38] P. Caprioglio, M. Stolterfoht, C. M. Wolff, T. Unold, B. Rech, S. Albrecht, D. Neher, *Adv. Energy Mater.* **2019**, *9*, 1901631.

[39] T. B. Song, Z. Yuan, F. Babbe, D. P. Nenon, E. Aydin, S. De Wolf, C. M. Sutter-Fella, *ACS Appl. Energy Mater.* **2020**, *3*, 2386.

[40] A. Al-Ashouri, A. Magomedov, M. Roß, M. Jost, M. Talaikis, G. Chistiakova, T. Bertram, J. A. Marquez, E. Kohnen, E. Kasparavicius, S. Levcenco, L. Gil-Escrig, C. J. Hages, R. Schlatmann, B. Rech, T. Malinauskas, T. Unold, C. A. Kaufmann, L. Korte, G. Niaura, V. Getautis, S. Albrecht, *Energy Environ. Sci.* **2019**, *12*, 3356.

[41] M. Chockalingam, N. Darwish, G. Le Saux, J. J. Gooding, *Langmuir* **2011**, *27*, 2545.

[42] M. D. Losego, J. T. Guske, A. Efremenko, J. P. Maria, S. Franzen, *Langmuir* **2011**, *27*, 11883.

[43] N. Phung, M. Verheijen, A. Todinova, K. Datta, M. Verhage, A. Al-Ashouri, H. Köbler, Xin Li, A. Abate, S. Albrecht, M. Creatore, *ACS Appl. Mater. Interfaces* **2022**, *14*, 2166.

[44] S. C. Watthage, Z. Song, N. Shrestha, A. B. Phillips, G. K. Liyanage, P. J. Roland, R. J. Ellingson, M. J. Heben, *ACS Appl. Mater. Interfaces* **2017**, *9*, 2334.

[45] Y. Du, C. Xin, W. Huang, B. Shi, Y. Ding, C. Wei, Y. Zhao, Y. Li, X. Zhang, *ACS Sustainable Chem. Eng.* **2018**, *6*, 16806.

[46] D. W. Ball, *Field Guide to Spectroscopy*, SPIE Press, Bellingham, WA **2006**, p. 68.

[47] T. Zhu, D. Zheng, J. Liu, L. Coolen, T. Pauporté, *ACS Appl. Mater. Interfaces* **2020**, *12*, 37197.

[48] F. Ansari, E. Shirzadi, M. Salavati-Niasari, T. LaGrange, K. Nonomura, J. Yum, K. Sivula, S. M. Zakeeruddin, M. K. Nazeeruddin, M. Grätzel, P. J. Dyson, A. Hagfeldt, *J. Am. Chem. Soc.* **2020**, *142*, 11428.

[49] S. Gharibzadeh, P. Fassl, I. M. Hossain, P. Rohrbeck, M. Frericks, M. Schmidt, T. Duong, M. R. Khan, T. Abzieher, B. Abdollahi Nejand, F. Schackmar, O. Almora, T. Feeney, R. Singh, D. Fuchs, U. Lemmer, J. P. Hofmann, S. A. L. Weber, U. W. Paetzold, *Energy Environ. Sci.* **2021**, *14*, 5875.

[50] Y. Qian, L. Li, H. Cao, Z. Ren, X. Dai, T. Huang, S. Zhang, Y. Qiu, L. Yang, S. Yin, *Adv. Funct. Mater.* **2023**, *33*, 2214731.

[51] J. C. de Mello, H. F. Wittmann, R. H. Friend, *Adv. Mater.* **2004**, *9*, 230.